Cross-correlation Between *Planck* CMB Lensing Potential and HELP Galaxy Catalogues

Chandra Shekhar Saraf[1] and Paweł Bielewicz[2]

1. Nicolaus Copernicus Astronomical Center, Polish Academy of Sciences, Bartycka 18, 00–716 Warsaw, Poland
2. National Center for Nuclear Research, Ludwika Pasteura 7, 02–093 Warsaw, Poland

Weak gravitational lensing of the Cosmic Microwave Background (CMB) contains information about the matter distribution in the Universe. Cross-correlation of CMB lensing with tracers of large scale structures like galaxies or quasars can be used to constrain the cosmological model of the Universe. We present the first study of the cross-correlation between Cosmic Microwave Background (CMB) lensing potential measured by the *Planck* satellite and $z \geq 0.8$ galaxies from the *Herschel* Extragalactic Legacy Project (HELP) photometric redshift catalogues. We use Maximum Likelihood Estimation to measure the galaxy linear bias, b, and the amplitude of cross-correlation, A, from a joint analysis of cross-power spectrum and galaxy auto-power spectrum. We find the amplitude A to be consistently lower than the expected value of unity for the standard cosmological model. We explore various tests and systematics to account for the observed discrepancy in the amplitude of cross-correlation.

1 Introduction

The Cosmic Microwave Background (CMB) is the oldest light that we can see in the Universe. Originating at redshift $z \simeq 1100$, the CMB offers a picture of the early Universe imprinted in temperature and polarization anisotropies. The precise measurements of the CMB (Planck Collaboration et al. 2020a; Planck Collaboration et al. 2020b; Planck Collaboration et al. 2020c) have helped us establish theories of large scale structure (LSS) and the standard model of cosmology.

CMB photons travelling towards us are deflected by the matter inhomogeneities encountered along their way. This distorts our picture of the early Universe and changes the observed statistical properties of the CMB anisotropies. However, these distortions carry integrated information about the matter distribution in the Universe all the way up to the last scattering surface.

Since gravitational lensing of the CMB is an integrated quantity, this lensing does not provide direct information about the evolution of large scale gravitational potential. The cross-correlation of the CMB lensing with traces of the LSS is useful to study the evolution and distribution of gravitational potential. It can also be used to constrain the evolution of dark energy on the onset of cosmic acceleration, study the dark matter density fluctuations, and constrain cosmological model of the Universe and models of structure formation.

In this work, we present the first study of the cross-correlation between the *Planck* CMB lensing convergence (Planck Collaboration et al., 2020c) and $z \geq 0.8$ photometric galaxy catalogue from the *Herschel* Extragalactic Legacy Project (HELP).

We estimate two parameters in this study: the galaxy linear bias, b and the amplitude of cross-correlation, A. We give a brief theoretical background in Sec. 2 and describe the data in Sec. 3. We present results of our analysis in Sec. 4 and discuss these results in Sec. 5.

2 Theory

We introduce a dimensionless lensing convergence κ defined as the 2D Laplacian of the lensing potential ϕ and its spherical harmonic counterpart as

$$\kappa(\hat{\mathbf{n}}) = -\frac{1}{2}\nabla^2\phi(\hat{\mathbf{n}}), \qquad \kappa_{\ell m} = -\frac{\ell(\ell+1)}{2}\phi_{\ell m}. \tag{1}$$

The theoretical angular power spectrum is computed under the Limber approximation (Limber, 1953) as

$$C_\ell^{xy} = \int_0^{\chi_*} d\chi \frac{W^x(\chi)W^y(\chi)}{\chi^2} P\left(k = \frac{\ell+1/2}{\chi}, z(\chi)\right), \tag{2}$$

where χ is the comoving distance, $\{x, y\} = \{\kappa, g\}$, $\kappa \equiv$ convergence and $g \equiv$ galaxy over-density and $P(k = \frac{\ell+1/2}{\chi}, z(\chi))$ is the matter power spectrum generated using CAMB[1] (Lewis et al., 2000). W^κ and W^g are lensing and galaxy over-density kernels, respectively, given by

$$W^\kappa(\chi) = \frac{3\Omega_\mathrm{m}}{2c^2} H_0^2 (1+z)\chi \frac{\chi_* - \chi}{\chi_*}, \tag{3}$$

$$\begin{aligned} W^g(\chi) = b\frac{H(\chi)}{c}\frac{dN}{dz(\chi)} + \\ + \frac{3\Omega_\mathrm{m}}{2c^2} H_0^2 (1+z)\chi \int_\chi^{\chi_*} d\chi' \frac{H(\chi')}{c}\left(1 - \frac{\chi}{\chi'}\right)(\alpha(\chi') - 1)\frac{dN}{dz(\chi')}\,, \end{aligned} \tag{4}$$

where c is the speed of light, Ω_m and H_0 are the present-day values of the matter density parameter and Hubble constant, respectively, χ_* is the comoving distance to the surface of the last scattering at redshift $z \simeq 1100$, $\frac{dN}{dz}$ stands for the redshift distribution of galaxies, and the second term in galaxy over-density kernel accounts for the gravitational magnification of background objects by foreground sources (magnification bias; Turner 1980). This effect depends on the slope, $\alpha(z)$, of the integral counts of sources above the flux threshold S, i.e., $N(>S) \propto S^{-\alpha}$. Because the slope estimated for objects selected from the HELP catalogue used in this work is $\alpha = 1$, the magnification bias term is null.

3 Data

3.1 CMB Lensing Data

We use the CMB lensing data from the 2018 *Planck* data release[2] described by Planck Collaboration et al. (2020c). The data package provides the spherical harmonic

[1] `https://camb.info/`

[2] `https://pla.esac.esa.int/#cosmology`

coefficients for the lensing convergence map, covering $\sim 67\%$ of the sky, derived from minimum-variance estimate of temperature and polarization data after mean-field subtraction along with the minimum-variance reconstruction of noise power spectrum $N_\ell^{\kappa\kappa}$. The spherical harmonic coefficients are provided in the HEALPix[3] (Górski et al., 2005) format with resolution $N_{\rm side} = 4096$. We downgrade these coefficients to $N_{\rm side} = 512$ before using in our analysis.

3.2 Galaxy Data

The *Herschel* Extragalactic Legacy Project (HELP) provides photometric redshifts of objects distributed over 23 extragalactic survey fields. The photometric catalogues contain objects observed between $0.36-4.5\mu m$ and cross-matched between 51 public surveys (Shirley et al., 2019). Some of these fields have inhomogeneous distribution of objects on the sky while some are very small in area, making them unsuitable for the cross-correlation studies. We choose three extragalactic fields, namely NGP, SGP, and the Herschel Stripe-82 (hereafter HS-82) for our analysis. The SGP field has two halves relatively different from one another in terms of density of objects. To avoid any effects coming from this inhomogeneity, we divide SGP in two parts. The physical properties of these four patches of the sky are given in Tab. 1. We select

Tab. 1: Physical properties of HELP patches. $N_{\rm obj}$ is the number of objects in each patch, $\overline{n}$ is the mean number of objects, and $f_{\rm sky}$ is the fraction of sky covered by patches.

Patch	area [deg^2]	$N_{\rm obj}$	$\overline{n}$ [gal pix^{-1}]	$\overline{n}$ [gal str^{-1}]	median z
NGP	179.14	102477	7.502	1.878×10^6	0.8859
HS-82	255.16	6255440	321.501	8.048×10^7	0.8871
SGP Part-1	85.83	3058179	467.254	1.170×10^8	0.9067
SGP Part-2	145.32	4358054	393.291	9.845×10^7	0.8776

objects with $z \geq 0.8$ and relative error on redshift, $\frac{\Delta z}{z} \leq 1.0$. We also apply two other filters, namely *flag-gaia* ≤ 2 and *stellarity* < 0.9 to remove point-like sources. After applying the mentioned filters, we have a total of ~ 13.8 million objects. We have orders of magnitude improvement on the mean density of objects over previous similar study performed (Bianchini et al., 2015).

We convert galaxy number count maps to galaxy over-density maps using the relation

$$g(\hat{\mathbf{n}}) = \frac{n(\hat{\mathbf{n}}) - \overline{n}}{\overline{n}}, \tag{5}$$

where $n(\hat{\mathbf{n}})$ is the number of objects in a given pixel and $\overline{n}$ is the mean number of objects per pixel. Figure 1 shows the galaxy over-density maps for all patches, from which we have filtered out $\ell \geq 400$. HELP also provides posteriors from the estimation of photometric redshifts. We stack these posteriors to form the redshift distribution of HELP patches.

[3] `https://healpix.jpl.nasa.gov/`

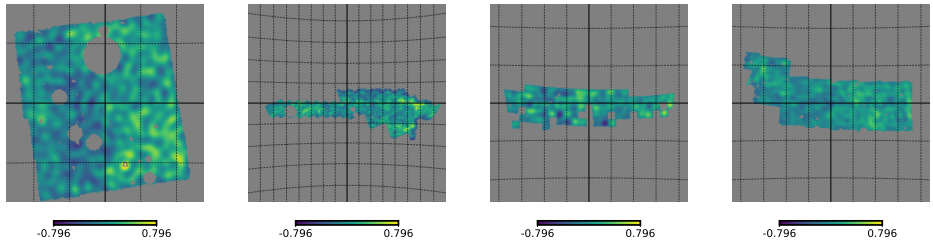

Fig. 1: Galaxy over-density maps of (from *left* to *right*): NGP, HS-82, SGP Part-1, and SGP Part-2 fields. Multipoles $\ell \geq 400$ have been filtered out from all maps.

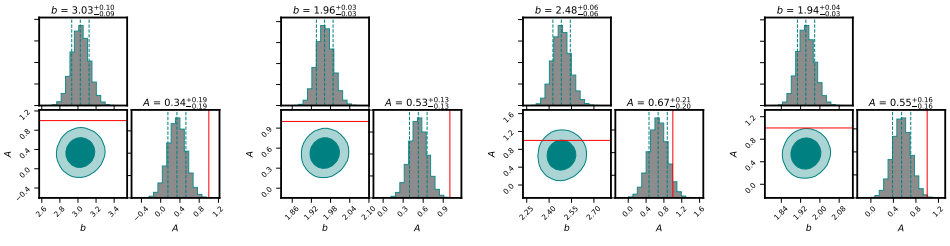

Fig. 2: Posteriors of estimated parameters for all HELP patches (NGP, HS-82, SGP Part-1 and Part-2, from *left* to *right*) with 68% and 95% confidence contours shown in darker and lighter shades, respectively. The three vertical lines are the median value of posterior and $\pm 1\sigma$ errors. The red line represents the value of $A = 1$ for standard ΛCDM.

4 Results

We implement the Maximum Likelihood technique for estimating parameters and use the publicly available package EMCEE (Foreman-Mackey et al., 2013) to sample the parameter space. The best-fit value of parameters obtained is the median of the posterior distribution after marginalizing over other parameters. The uncertainties on these parameters are the 16^{th} and 84^{th} percentile of the posterior. In Fig. 2 the posteriors for estimated parameters is shown with 1σ errors shown by vertical dashed lines. The red line corresponds to $A = 1$, which is the value expected for the standard ΛCDM model. We find that in all cases there is a significant deviation of measured amplitude A from the expected value of 1. We explore some possible reason for this discrepancy in the next section.

5 Discussion and Conclusions

5.1 Catastrophic photometric redshift error rates

Catastrophic photometric error rates account for the misestimation of true value of redshift by a significant amount. The rate and outcome of catastrophic errors depend on the number of photometric filters and their relation to the spectral features that carry principal information about the redshift (Muir & Huterer, 2016). We randomly assign redshifts for a fraction x of galaxies in the HELP catalogue to

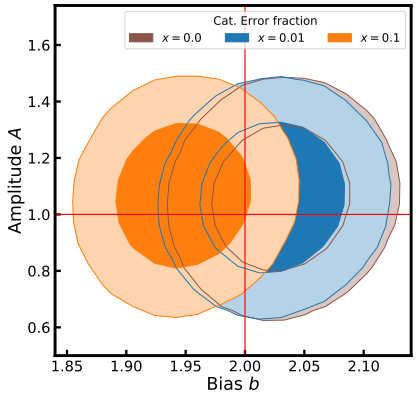

Fig. 3: Effect of catastrophic errors on amplitude A and galaxy bias b for $x = 0$ (no catastrophic errors), $x = 0.01$ and $x = 0.1$ catastrophic error rate. The red lines represent the true values of b and A used in simulations ($b = 2$ and $A = 1$).

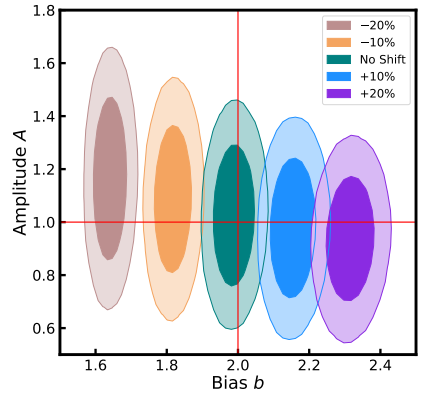

Fig. 4: Effect of shifting median redshift in theoretical power spectrum on cross-correlation amplitude A and galaxy bias b. The red lines represent the true values of b and A used in simulations ($b = 2$ and $A = 1$).

model catastrophic errors. We choose $x = 0.01$ and $x = 0.1$ which roughly amounts to the lower and upper limits, respectively, of the fraction achieved in current surveys. Figure 3 shows contour plots in $A - b$ plane for simulated SGP Part-2 field corresponding to $x = 0.01$ and 0.1. We notice that different fractions of catastrophic errors have no significant effect on the amplitude of cross-correlation A.

5.2 Median redshift

In this section we examine the effect of shifting the median redshift which may be misestimated due to some systematics. We model the redshift distribution of HELP fields using a function of the form

$$\frac{dN}{dz} = a_0 z^{a_1} \exp\left[- \left(\frac{z}{a_2} \right)^{a_3} \right], \tag{6}$$

where parameter a_2 serves as a proxy for the median redshift. In Fig. 4 we explore the effect on shifting the median redshift from -20% to $+20\%$ using simulations for SGP Part-2 field. We notice that the amplitude of cross-correlation favours a higher value when the median redshift is shifted towards lower values. However, shifts of $15-20\%$ in the median redshift is very extreme and may not be physically realizable.

5.3 Contamination from low-z objects

The photometric redshift of objects have uncertainties associated with them, due to which objects with true redshift from $z < 0.8$ can have estimated photometric redshift $z \geq 0.8$. It can lead to significant contamination of our sample by low redshift objects. To study this effect, we estimate parameters without any redshift cut (Saraf et al., 2022). Since the resulting redshift distribution will be broader, we

assume a redshift dependent galaxy bias of the form

$$b = b_0(1 + z). \tag{7}$$

Table 2 compares the parameters estimated with redshift cut at $z = 0.8$ and without any redshift cut. There is clear and significant improvement in the amplitude of the cross-correlation by roughly 1σ.

Tab. 2: Comparison of parameters estimated with redshift cut applied to objects at $z = 0.8$ and without any redshift cut.

Patch	$z \geq 0.8$		No $z-$cut	
	b	A	b_0	A
NGP	$3.03^{+0.10}_{-0.09}$	$0.34^{+0.19}_{-0.19}$	$0.87^{+0.01}_{-0.01}$	$0.51^{+0.21}_{-0.21}$
HS-82	$1.96^{+0.03}_{-0.03}$	$0.53^{+0.13}_{-0.13}$	$0.79^{+0.01}_{-0.01}$	$0.73^{+0.14}_{-0.13}$
SGP Part-1	$2.48^{+0.06}_{-0.06}$	$0.67^{+0.21}_{-0.20}$	$0.98^{+0.02}_{-0.02}$	$0.86^{+0.21}_{-0.21}$
SGP Part-2	$1.94^{+0.04}_{-0.03}$	$0.55^{+0.16}_{-0.16}$	$0.66^{+0.01}_{-0.01}$	$0.70^{+0.17}_{-0.17}$

6 Summary

In this work, we presented the first study of cross-correlation between *Planck* CMB lensing convergence and $z \geq 0.8$ photometric galaxy catalogue of three HELP fields, NGP, SGP, and HS-82. We estimate the galaxy linear bias and the amplitude of cross-correlation and find that the amplitude is consistently smaller than the expected value of 1 for all HELP fields used in our analysis. We investigated some possible systematics that can account for this discrepancy. We find that the catastrophic photometric errors have no notable effect on the amplitude. We also investigate the effect of shifting the median redshift of the distribution which leads to an increase in the amplitude when the median redshift is shifted to lower values by $15 - 20\%$. But such extreme shifts may not be physically possible. We further take into account possible contamination from low-z sources by estimating the parameters without any redshift cut and find a 1σ increase in the amplitude. A detailed study of parameters without any redshift cut can be found in Saraf et al. (2022).

Acknowledgements. The authors thank Raphael Shirley, Kenneth Duncan, and Katarzyna Małek for their help with different aspects of HELP data. We also thank Federico Bianchini and Agnieszka Pollo for valuable comments and discussions.

References

Bianchini, F., et al., *ApJ* **802**, 1, 64 (2015)

Foreman-Mackey, D., Hogg, D. W., Lang, D., Goodman, J., *PASP* **125**, 925, 306 (2013)

Górski, K. M., et al., *ApJ* **622**, 2, 759 (2005)

Lewis, A., Challinor, A., Lasenby, A., *ApJ* **538**, 2, 473 (2000)

Limber, D. N., *ApJ* **117**, 134 (1953)

Muir, J., Huterer, D., *Phys. Rev. D* **94**, 4, 043503 (2016)

Planck Collaboration, et al., *A&A* **641**, A1 (2020a)

Planck Collaboration, et al., *A&A* **641**, A6 (2020b)

Planck Collaboration, et al., *A&A* **641**, A8 (2020c)

Saraf, C. S., Bielewicz, P., Chodorowski, M., *MNRAS* **515**, 2, 1993 (2022)

Shirley, R., et al., *MNRAS* **490**, 1, 634 (2019)

Turner, E. L., *ApJL* **242**, L135 (1980)